Symplectic Ray Tracing: A New Frontier in Non-linear Ray Tracing

Tetsu R. Satoh
Communications Research Laboratory
2-2-2 Hikaridai, Seika, Soraku,
619-0237, Kyoto, JAPAN
tetu-s@crl.go.jp

ABSTRACT

This paper describes a method of *symplectic ray tracing* for visualizing non-linear dynamical systems. Symplectic ray tracing is simply an extended version of the ray tracing techniques commonly used to generate computer graphics. However, high performance in analyzing non-linear dynamical systems is achieved by applying Hamiltonian dynamics, symplectic numerical integration, and automatic differentiation. The key characteristics of this method are the capability to simulate any number of dimensions, numerical error estimation, and code re-usability. This paper also demonstrates some visualization results for non-linear optical phenomena computed by symplectic ray tracing.

Keywords

Symplectic Integration, Automatic Differentiation, Non-linear Ray Tracing

1. INTRODUCTION

Non-linear ray tracing is a natural extension of traditional ray tracing for visualizing non-linear phenomena. Black hole space-time has been visualized [Yam89][Nol96][Wei00][Kob01] by calculating the paths of light rays according to Einstein's general theory of relativity [Mis73]. Inhomogeneous space has been visualized [Sai93][Sta96] by applying geometric optics. Equations of dynamical systems and other general curves have been utilized to describe curved light rays [Grö95], while multi-layer approximation of the space has been used to visualize mirages and Newtonian rings [Ber90][Dia94][Hir99].

However, some problems remain. First, no general approach to visualizing these phenomena has yet been proposed. For each problem, a different method has been required. Second, accuracy of calculation results is not guaranteed because in conventional studies, the classical Runge-Kutta method has been used to solve the differential equations of light rays. The method causes accumulation of numerical errors for calculating the flow of dynamical systems in long-term.

The author thus proposes a unique method to overcome such problems by integrating ray tracing [Whi80], Hamiltonian dynamics [Gol80], symplectic numerical integration [San91][Yos93], and automatic differentiation [Gri89][Iri88].

Symplectic numerical integration for Hamiltonian dynamics has been developed by mathematicians and physicists over the last few decades, but it has not been applied to computer graphics. This paper demonstrates that symplectic numerical analysis is well suited to ray tracing simulation of various optical phenomena.

2. NON-LINEAR RAY TRACING

In this section, a process and its problem for extending traditional (linear) ray tracing to non-linear ray tracing are presented. The following is a typical procedure of non-linear ray tracing. This algorithm is commonly used in almost all related works.

1. Fix the location of an observer (the eye in Fig. 1);
2. fix the view screen of the observer (the center plane in the figure);
3. trace the light rays until they cross the object (the dotted curves indicate light rays);
4. obtain the color on the object surface at the crossing point (the left plane indicates the object);

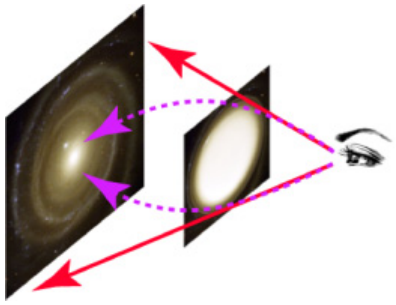

Figure 1: Model of non-linear ray tracing. The human eye on the right represents an observer, and the galaxies at the left represents an object arranged in space. Although the non-linear light rays travel along the dotted curves, the human eye perceives the paths of the rays as solid lines. As a result, the observer sees a warped image, indicated by the illustration on the center.

5. render a pixel according to the color.

The main problem with this approach are as follows.

(a) For calculating the paths of light rays, which physical models and equations should be introduced?

(b) Which method should be introduced to solve the equations? (The equations are typically non-linear differential equations)

First of all, conventional ray tracing employs straight lines to calculate the paths of light rays. The equation of a straight line is given here in vector form:

$$\mathbf{r} = \mathbf{a} + s\mathbf{v} \tag{1}$$

where $\mathbf{a}$ is a starting point, $\mathbf{v}$ is a direction vector and s is a parameter. Equation (1) can be rewritten as follows for the components of the vectors:

$$x_i = a_i + sv_i \tag{2}$$

where x_i is a component of vector $\mathbf{r}$. By differentiating twice, Eq. (2) can be rewritten as a form of differential equation:

$$\frac{d^2x^i}{ds^2} = 0. \tag{3}$$

Traditional ray tracing is thus a rendering technique in which the path of a light ray is calculated by solving Eq. (3).

In an inhomogeneous transparent object, the equation for a light rays is given by

$$\frac{dn}{ds}\frac{dx^i}{ds} + n\frac{d^2x^i}{ds^2} = \frac{\partial n}{\partial x^i}, \tag{4}$$

where n is the refractive index and the other variables are the same as in Eq. (3). Equation (4) is derived from the Fermat's principle in geometric optics. When n is constant, Eq. (4) reduces to Eq. (3).

In black-hole space-time, the equation for a light ray is given by

$$\frac{d^2x^i}{ds^2} + \Gamma^i_{kl}\frac{dx^k}{ds}\frac{dx^l}{ds} = 0, \tag{5}$$

where Γ^i_{kl}, called the Christoffel symbol, is a function used to calculate the curvature of space and the other variables are again the same as in Eq. (3). Equation (5) is known as the geodesic equation. When the gravitational force of a black hole is very weak, Γ^i_{kl} becomes zero and Eq. (5) also reduces to Eq. (3).

As shown above, past studies have adopted equations such as the geodesic equation, the Helmholtz equation, the Eikonal equation, and so on. However, from a mathematical viewpoint, we know that most such equations can be represented in terms of Hamilton's canonical equation:

$$\begin{cases} \dfrac{dp_i}{ds} &= -\dfrac{\partial H}{\partial q_i} \\ \dfrac{dq_i}{ds} &= \dfrac{\partial H}{\partial p_i} \end{cases}, \tag{6}$$

where q_i indicates the location component , p_i indicates the momentum of q_i , and H is a Hamiltonian constructed from q_i and p_i. One purpose of this paper is to generalize non-linear ray tracing by applying Eq. (6). Since this equation is applicable to a great many types of dynamical systems, this approach can be used to solve problem (a).

To solve differential equations that describe a dynamical system numerically, the classical Runge-Kutta method has been used widely in past studies. The classical fourth order Runge-Kutta method is very popular and applicable to solving any differential equation. However, it does not account for the properties of the differential equations to be solved, and the accuracy of the results is not guaranteed. Thus, in this paper, the author introduces symplectic numerical integration to solve Hamilton's canonical equation. Because symplectic numerical integration considers the so-called "symplecticness", which is a property of canonical map preserving invariants, good numerical results can be obtained[Hai02]. In other words, existence of suitable method for solving the equation can be used to overcome problem (b).

3. GEOMETRIC OPTICS BY HAMILTONIAN DYNAMICS

In accordance with Hamiltonian dynamics, the equations of motion of a light ray are obtained from a scalar function, which is referred to as a Hamiltonian. For example, the Hamiltonian that describes the uniform motion of a particle in three-dimensional space is given as

$$H = \frac{1}{2}\left(p_x^2 + p_y^2 + p_z^2\right) \tag{7}$$

where (p_x, p_y, p_z) denotes momentum of the particle. Since Eq. (7) leads to equations of a straight line, we can introduce Eq. (7) as the Hamiltonian for calculating the paths of light rays in ordinary flat space. In other words, the Hamiltonian of Eq. (7) can be applied to a conventional ray tracing.

In an inhomogeneous transparent object such as a quantity of air above the ground, the Hamiltonian is given as

$$H = \frac{1}{2} n(x, y, z)(p_x^2 + p_y^2 + p_z^2), \tag{8}$$

where $n(x, y, z)$ is the refractive index at point (x, y, z). For example, when the temperature increases with increasing height above the earth's surface, the path taken by a light ray in the atmosphere is as shown in Fig. 2a [Ber90]. This phenomenon can be simulated by the Hamiltonian of Eq. (8) as shown in Fig. 2b. In numerical simulation with this Hamiltonian, the light rays are traced in 6-dimensional phase space: Three components are location coordinates and the other three are for the momentum. Note that the momentum components are not used for rendering on the display.

From the general theory of relativity, the Hamiltonian for spherically symmetrical black-hole space-time is given as

$$\begin{aligned} H &= \left(1 - \frac{r_g}{r}\right)^{-1} \frac{{p_t}^2}{2} - \left(1 - \frac{r_g}{r}\right) \frac{{p_r}^2}{2} \\ &\quad - \frac{{p_\theta}^2}{2r^2} - \frac{{p_\phi}^2}{2r^2 \sin^2 \theta}, \end{aligned} \tag{9}$$

where (t, r, θ, ϕ) are the components of a set of four-dimensional polar coordinates, $(p_t, p_r, p_\theta, p_\phi)$ denotes the corresponding momentum components, and r_g, which is referred to as the black-hole radius, corresponds to the mass of the black hole. The paths of the light rays in this case according to the Hamiltonian are shown in Fig. 3. This illustrates the so-called "gravitational lens" effect. The difference between a gravitational lens and an optical lens is that the gravitational lens has no focus. More generally, the following formula can be used to derive other Hamiltonians for black-hole space-time. For any answer g^{ij} of the Einstein equation,

$$H = \frac{1}{2} \sum_{i,j=0}^{3} g^{ij} p_i p_j \tag{10}$$

is a Hamiltonian for the light rays.

Above mentioned Hamiltonians can be used for non-linear ray tracing. By partially differentiating each Hamiltonian, we can obtain the equation of motion of non-linear light rays. However, obtaining partial differentials for all components is troublesome work. Moreover, the resulting form of Hamilton's canonical equation can not always be solved analytically. Next section gives how to overcome such problems by numerical computation.

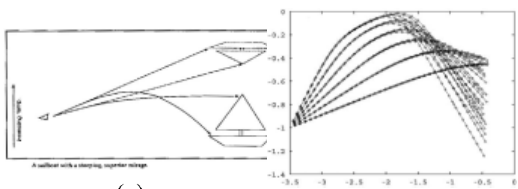

(a) (b)

Figure 2: (a) Path taken by light rays when the temperature increases with increasing height above earth's surface (illustrated by Berger [Ber90]). (b) This phenomenon is simulated by the Hamiltonian.

4. SYMPLECTIC INTEGRATION AND AUTOMATIC DIFFERENTIATION

Symplectic integration[San91][Yos93] is a numerical methods specifically designed for solving Hamilton's canonical equation. Over the last two decades, this method's usefulness has been confirmed in many scientific fields. The essence is to preserve conserved physical quantities such as the total energy of a system.

One of the simplest symplectic solvers is the following implicit Euler method:

$$\begin{cases} p_{k+1} &= p_k - \tau \dfrac{\partial H(p_k, q_{k+1})}{\partial q} \\ q_{k+1} &= q_k + \tau \dfrac{\partial H(p_k, q_{k+1})}{\partial p} \end{cases}, \tag{11}$$

where τ is the step size of the numerical approximation. The implicit Euler method has first-order numerical accuracy, which is lower than the fourth-order accuracy of the classical Runge-Kutta method. However, the symmetric decomposition [Yos90] or fractal decomposition [Suz84] method can be used to construct an accurate formula of any order from the first-order implicit Euler method. A fourth-order implicit symplectic intergrator, which is constructed from the implicit Euler method by applying the symmetric decomposition method, is used to solve the differential equations in this paper.

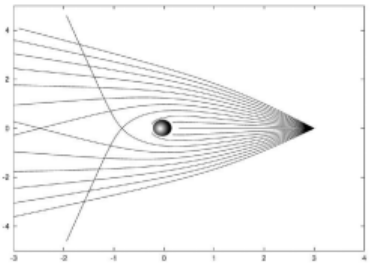

Figure 3: Paths of light rays subject to the gravitational convex lens effect.

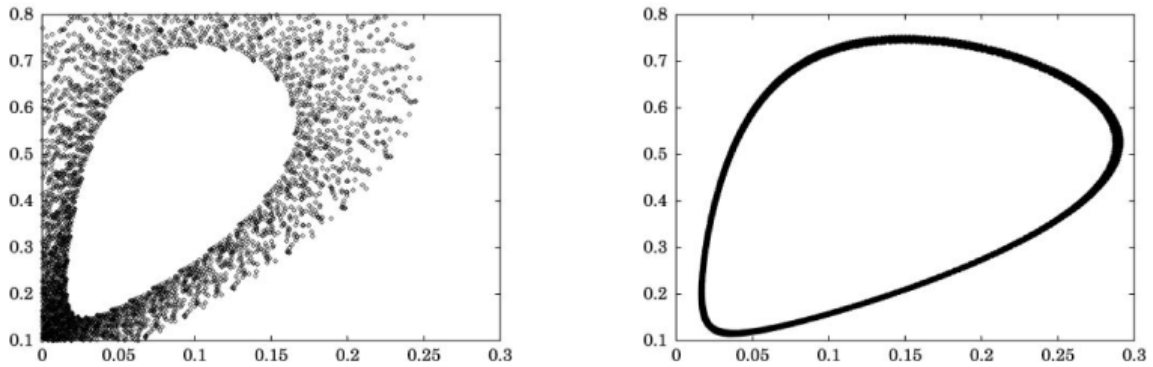

Figure 4: Left: classical Runge-Kutta method used to solve Hamilton's canonical equation. The orbits of the photons produce a divergent curve. Right: symplectic method used to solve same canonical equation. The orbits of the photons produce a closed curve. The analytical solution of Hamilton's canonical equation indicates the correctness of the graph on the right.

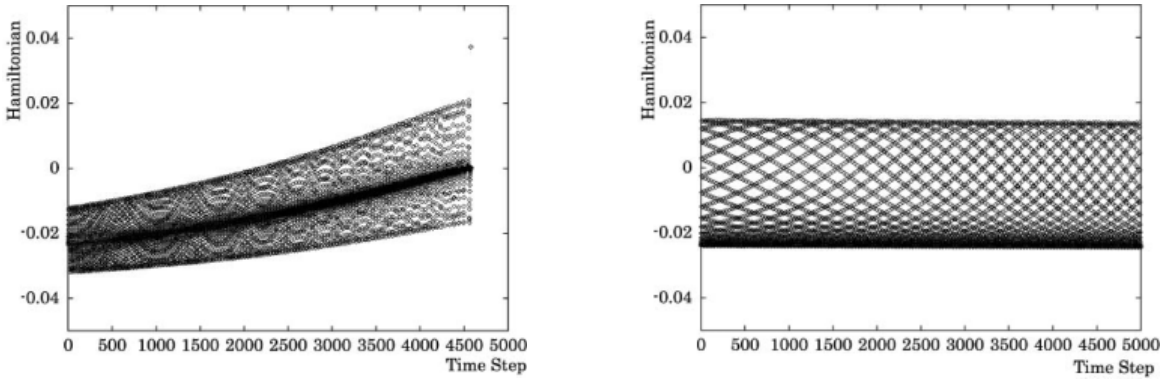

Figure 5: Left: value of the Hamiltonian obtained by the classical Runge-Kutta method. The Hamiltonian increases with each time step. After 4500 time steps, the Hamiltonian continues to infinity with accumulated numerical errors. Right: value of the Hamiltonian obtained by the symplectic numerical method. The Hamiltonian does not diverge, as long as slight vibrations are assumed negligible.

Figure 4 shows a very simple example comparing symplectic and non-symplectic solvers. Each curve in the $(p-q)$ plane indicates the orbit of a light ray for the case in which $H = pq(p+q-1)$. The left graph shows the result obtained by the classical fourth-order Runge-Kutta method while the right figure shows that obtained by the implicit fourth-order symplectic method. Since analytical solutions of the equation give closed curves [Nak94], the right figure should be a correct result. Figure 5 shows the values of the Hamiltonian that have to be preserved. For the left graph, the Hamiltonian increased with each time step and after the number of time steps reached 4500, the Hamiltonian continued to infinity with accumulated numerical errors. For the right graph, the Hamiltonian did not diverge as long as slight vibrations could be assumed negligible.

In this test case, the form of the Hamiltonian is very simple, so it appears that there are no problem with the symplectic numerical method. However, it is hard to apply the formula of Eq. (11) to a complex Hamiltonian. This is because implementing the symplectic method requires all the derivatives of the Hamiltonian. For example, the Hamiltonian in axisymmetric space-time is given as

$$H = \left(1 + \frac{r_g r(a^2+r^2)}{\rho^2\Delta}\right)\frac{{p_t}^2}{2} - \frac{\Delta}{\rho^2}\frac{{p_r}^2}{2} - \frac{1}{\rho^2}\frac{{p_\theta}^2}{2} - \frac{\rho^2 - r_g r}{\rho^2\Delta\sin^2\theta}\frac{{p_\phi}^2}{2} + \frac{a r_g r}{\rho^2\Delta}p_t p_\phi, \quad (12)$$

where a corresponds to the angular momentum of the black hole, $\rho^2 \equiv r^2 + a^2\cos^2\theta$, and $\Delta \equiv r^2 - r_g r + a^2$. For the above Hamiltonian, *Mathematica* outputs the derivative with respect to θ as follows:

$$\begin{aligned} D[H,\theta] \;=\; & \frac{2p_\phi p_t r r_g \cos\theta\sin\theta a^3}{(a^2+r^2-rr_g)(r^2+a^2\cos^2\theta)^2} \\ & - \frac{{p_\phi}^2(r^2 - r_g r + a^2\cos^2\theta)\cot\theta a^2}{(a^2+r^2-rr_g)(r^2+a^2\cos^2\theta)^2} + \\ & \frac{{p_\phi}^2\cot\theta a^2}{(a^2+r^2-rr_g)(r^2+a^2\cos^2\theta)} \\ & - \frac{{p_\theta}^2\cos\theta\sin\theta a^2}{(r^2+a^2\cos^2\theta)^2} - \end{aligned}$$

$$\frac{{p_r}^2(a^2+r^2-rr_g)\cos\theta\sin\theta a^2}{\left(r^2+a^2\cos^2(\theta)\right)^2}+$$
$$\frac{{p_t}^2 r(a^2+r^2)r_g\cos\theta\sin\theta a^2}{(a^2+r^2-rr_g)(r^2+a^2\cos^2\theta)^2}+$$
$$\frac{{p_\phi}^2(r^2-r_g r+a^2\cos^2\theta)\cot\theta\csc^2\theta}{(a^2+r^2-rr_g)(r^2+a^2\cos^2\theta)}.$$

Implementation of such a complicated expression would lead to mistakes and a slow computation speed. The author's solution to this problem is to employ *fast automatic differentiation techniques* [Gri89] [Iri88]. In this approach, we define a vector $(f(p,q), \partial_p f(p,q), \partial_q f(p,q))$. We also define the operations of the vector. For example, addition and multiplication are defined as follows:

$$\begin{aligned}&(f,\partial_p f,\partial_q f)+(g,\partial_p g,\partial_q g)\\ &\quad=\ (f+g,\partial_p f+\partial_p g,\partial_q f+\partial_q g)\\ &(f,\partial_p f,\partial_q f)\times(g,\partial_p g,\partial_q g)\\ &\quad=\ (fg,\partial_p f\times g+f\times\partial_p g,\partial_q f\times g+f\times\partial_q g)\end{aligned}$$

We now give an example of the calculation. For a Hamiltonian $H=pq$, fast automatic differentiation calculates

$$\begin{aligned}&(p,1,0)\times(q,0,1)\\ =\ &(p\times q,\partial_p p\times q+p\times\partial_p q,\partial_q p\times q+p\times\partial_q q)\\ =\ &(pq,1\times q+p\times 0,0\times q+p\times 1)\\ =\ &(pq,q,p)\\ =\ &(H,\partial_p H,\partial_q H).\end{aligned}$$

As shown above, the operations and partial differentiations are calculated simultaneously without truncation errors.

5. IMPLEMENTATION AND VISUALIZATION EXAMPLES

In symplectic ray tracing, an "n-dimensional ray-tracing" means a tracing of light rays in $2n$-dimensional space-time, constructed with n location components and n momentum components. For example, a 1-dimensional symplectic ray tracing traces light rays in 2-dimensional phase space.

Ordinary ray tracing: 3- or 4-dimensional case

The Hamiltonian for ordinary space is given by Eq. (7). According to the special theory of relativity, Eq. (7) can be extended to four dimensional space-time in the form:

$$H=\frac{1}{2}(p_x^2+p_y^2+p_z^2-p_t^2), \qquad (13)$$

where p_t indicates the momentum of time. In polar coordinates, the Hamiltonian takes the form:

$$H=\frac{1}{2}(p_r^2+\frac{1}{r^2}p_\theta^2+\frac{1}{r^2\sin^2\theta}p_\phi^2-p_t^2), \qquad (14)$$

where (p_r,p_θ,p_ϕ) denotes the momentums for polar coordinates (r,θ,ϕ). Equations (7), (13), and (14) are for light rays traveling straightforwardly through the space. These Hamiltonians yield the result illustrated in Fig. 6. The original picture in Fig. 6 was taken by NASA's Hubble Space Telescope [1] (credit: D. Figer and NASA).

Black-hole space-time: 4-dimensional case

In this section, black-hole space-time refers to a four-dimensional space with a black hole at the origin. According to the general theory of relativity, we derive the Hamiltonian for spherically symmetrical space-time:

$$\begin{aligned}H\ =\ &\left(1-\frac{r_g}{r}\right)^{-1}\frac{{p_t}^2}{2}-\left(1-\frac{r_g}{r}\right)\frac{{p_r}^2}{2}\\ &-\frac{{p_\theta}^2}{2r^2}-\frac{{p_\phi}^2}{2r^2\sin^2\theta},\end{aligned} \qquad (15)$$

where (t,r,θ,ϕ) denotes the components of a set of four-dimensional polar coordinates, $(p_t,p_r,p_\theta,p_\phi)$ denotes the corresponding momentum components, and r_g, which is referred to as the black-hole radius, corresponds to the mass of the black hole. The Hamiltonian of Eq. (15) generates the result shown in Fig. 7a. This phenomenon is known as the gravitational convex lens effect. When an observer turn his or her face toward the opposite direction from the black hole, the gravitational concave lens effect, which is illustrated in Fig. 7b, is observed. This case shows that the whole universe is observed at a location close to the black hole, positioned to the rear of the observer. The full details of both visualization results have been given by, for example, Nemiroff's paper [Nem92] with computer-generated illustrations.

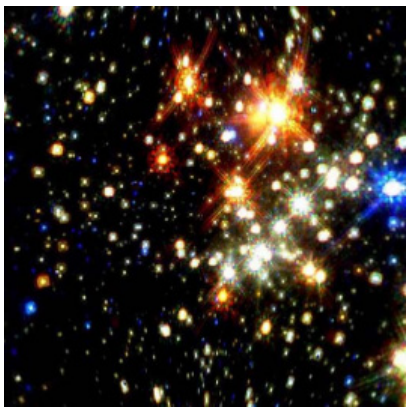

Figure 6: Symplectic ray tracing example for flat, ordinary space-time.

[1] http://oposite.stsci.edu/pubinfo/pr/1999/30/index.html

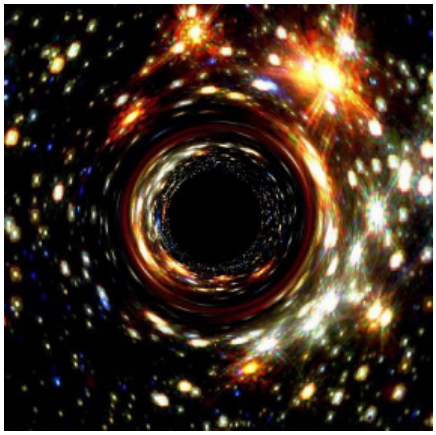

(a)

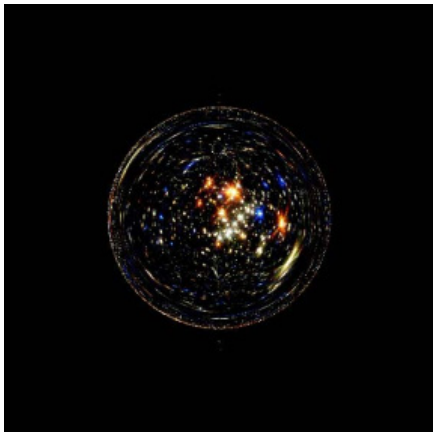

(b)

Figure 7: (a) Visualization example for a spherically symmetrical black hole. The bright galaxies are warped by the huge gravitation of the black hole. (b) Visualization example for the gravitational concave lens effect. The image shows that the whole universe is observed at a location close to the black hole, positioned to the rear of the observer.

Figure 8 is an example by using colors, texture, and volume rendering. The background image shows global information, and some of the objects show local information. The transparent board is rendered by a volume rendering technique taking into account the gravitational force. As shown in this case, symplectic ray tracing inherits many techniques from conventional ray tracing.

Mirages: 3-dimensional case

For simulation in 3-dimensional space-time, we construct a world model with an omni-directional image as shown in Fig. 9a. This image was taken by the HyperOmniVision [Yam93], which is an omni-directional camera (Fig. 9b). In inhomogeneous transparent objects such as a quantity of air above

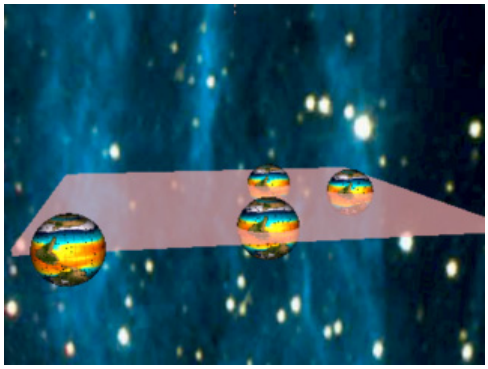

(a)

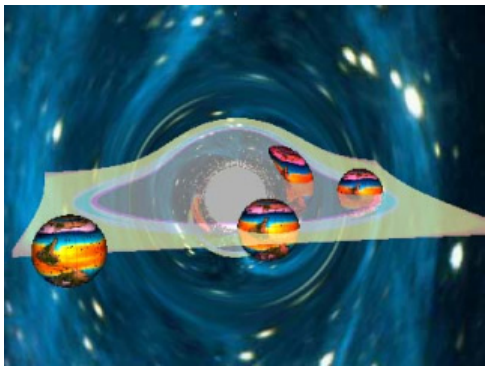

(b)

Figure 8: Information visualization based on texture mapping, color, and volume rendering. (a) The spacetime contains no black hole. (b) The spheres and the board are colored by taking into account the gravitational force.

the ground, the Hamiltonian is given as

$$H = -\frac{1}{2}n(x,y,z)(p_x^2 + p_y^2 + p_z^2), \qquad (16)$$

where $n(x,y,z)$ is the refractive index at point (x,y,z). The equation of motion derived from Eq. (16) is mathematically equivalent to Eq. (4). When $n = 1$, Eq. (16) generates the result shown in Fig. 10a. This is a normal view of a park in Nara, Japan, without the mirage.

On the earth, the function of the refractive index can take many forms. For example, when the temperature decreases with increasing height, the function can be modeled as [Sai93]:

$$n = 0.85 - 0.3z^3 + 0.03\cos(3\pi x). \qquad (17)$$

Some kinds of mirages have been classified and visualized [Ber90]. Equation (16) is applicable to visualizing all of them. A visualization example is shown in Fig. 10b. Light rays curved by mirages generates this strange picture. With a drastic increase in the ground temperature, the surface of the earth behaves like a mirror.

(a) (b)

Figure 9: (a) Omni-directional image. (b) An omni-directional camera, "HyperOmniVision".

Figure 11 shows another kind of mirage. In this case, the function of the refractive index is modeled as:

$$n = 0.85 + 1.3(z + 1.2)^3 + 0.03\cos(3\pi x). \quad (18)$$

There is a deer at the bottom of Fig. 11a, while in Fig. 11b, there is a deer at the bottom and a ghost of the deer at the top. This mirage, called Vince's phenomenon, is caused when air near the ground is cooler than the air higher up.

6. CONCLUSION

The author has introduced the concept of symplectic ray tracing, a new approach to visualizing natural phenomena. Symplectic ray tracing enables local error estimation, global numerical error control, and quick implementation by employing Hamiltonian dynamics and symplectic numerical analysis. This paper has demonstrated the numerical accuracy of this approach by a simple test and produced rendering results. The proposed method could be used to visualize phenomena based on non-linear light rays with high accuracy for long-term computation. Although this method cannot be applied to phenomena that are not described by a Hamiltonian, it does provide sufficient generality for visualizing natural phenomena.

7. ACKNOWLEDGMENTS

The author thanks the members of the Mathematical Science Mailing-list[2] for many discussions and suggestions.

8. REFERENCES

[Ber90] Berger, M., Trout, T. and Levit, N.: Ray Tracing Mirages, *IEEE CG & A.*, Vol. 10, No. 3, pp. 36–41, 1990.

[Dia94] Dias, M. L.: Ray Tracing Interference Color: Visualizing Newton's Rings, *IEEE CG & A.*, Vol. 14, No. 3, pp. 17–20, 1994.

[Gol80] Goldstein, H.: *Classical Mechanics 2nd ed.*, Addison-Wesley Publishing Company Inc., 1980.

[Gri89] Griewank, A.: On Automatic Differentiation, *Mathematical Programming: Recent developments and Applications*, pp. 83–108, 1989.

[Grö95] Gröller, E.: Nonlinear Ray Tracing: Visualizing Strange Worlds, *The Visual Computer*, Vol. 11, pp. 263–274, 1995.

[Hai02] Hairer, E., Lubich, C. and Wanner, G.: *Geometric Numerical Integration–Structure-Preserving Algorithms for Ordinary Differential Equations*, Springer-Verlag Berlin Heidelberg, 2002.

[Hir99] Hirayama, H., Kaneda, K., Yamashita, H., Yamaji, Y. and Monden, Y.: Visualization of Optical Phenomena Caused by Multilayer Films with Complex Refractive Indices, *Proc. Pacific Graphics 1999*, pp. 128–137, 1999.

[Iri88] Iri, M., Tsuchiya, T. and Hoshi, M.: Automatic Computation of Partial Derivatives and Rounding Error Estimates with Applications to Large-Scale Systems of Nonlinear Equations, *J. Computational and Applied Mathematics*, Vol. 24, pp. 365–392, 1988.

[Kob01] Kobras, D., Weiskopf, D. and Ruder, H.: Image-Based Rendering and General Relativity, *Proc. WSCG Conf.*, pp. 130–137, 2001.

[Mis73] Misner, C. W., Thorne, K. S. and Wheeler, J. A.: *Gravitation*, W. H. Freeman and Co., 1973.

[Nak94] Nakamura, Y. and Hashimoto, T.: On the Discretization of the Three-Dimentional Volterra System, *Physics letters A*, Vol. 193, pp. 42–46, 1994.

[Nem92] Nemiroff, R. J.: Visual Distortions near a Neutron Star and Black Hole, *American J. Physics*, Vol. 61, No. 7, pp. 619–632, 1992.

[Nol96] Nollert, H. P., Kraus, U. and Ruder, H.: Visualization in Curved Spacetimes. I. Visualization of Objects via Four-Dimensional Ray-Tracing, in *Relativity and Scientific Computing*, Springer-Verlag Berlin, 1996.

[2] http://www.mathsci.org/

(a) (b)

Figure 10: (a) Picture of a park in Nara, Japan, without a mirage. (b) Visualization example of a mirage in the same park. The y-axis is perpendicular to the ground, and the camera is positioned at the point x=-3.5, y=0.

(a) (b)

Figure 11: Another kind of mirage. (a) There is a deer at the bottom of the picture. (b) A ghost of the deer appears at the top. The y-axis is perpendicular to the ground, and the camera is positioned at the point x=-3.5, y=-1.

[Sai93] Saito, Y., Makino, M. and Oishi, S.: A Ray Tracing Algorithm for Anisotropic Inhomogeneous Transparency Objects, *Trans. IEICE*, Vol. J76-D-II, No. 8, pp. 1755–1762, 1993, (in Japanese).

[San91] Sanz-Serna, J.: Symplectic Intergrators for Hamiltonian Problems: An Overview, *Acta Numerica*, pp. 243–286, 1991.

[Sta96] Stam, J. and Languénou, E.: Ray Tracing in Non-Constant Media, *Proc. 7th Eurographics Workshop on Rendering*, pp. 225–234, 1996.

[Suz84] Suzuki, M.: Decomposition Formulas of Exponential Operators and Lie Exponentials with Some Applications to Quantum Mechanics and Statistical Physics, *J. Math. Phys.*, Vol. 26, No. 4, pp. 601–612, 1984.

[Wei00] Weiskopf, D.: Four-Dimensional Non-Linear Ray Tracing as a Visualization Tool for Gravitational Physics, *Proc. IEEE Visualization 2000*, pp. 445–448, 2000.

[Whi80] Whitted, T.: An Improved Illumination Model for Shaded Display, *Commun. ACM*, Vol. 23, No. 6, pp. 343–349, 1980.

[Yam89] Yamashita, Y.: Computer Graphics of Blackhole: Extension of Raytracing to Curved Four-Dimensional Space-Time, *Trans. Information Processing Society of Japan*, Vol. 30, No. 5, pp. 642–651, 1989, (in Japanese).

[Yam93] Yamazawa, K., Yagi, Y. and Yachida, M.: Omnidirectional Imaging with Hyperboloidal Projection, *Proc. Int. Conf. on Intelligent Robots and Systems*, Vol. 2, pp. 1029–1034, 1993.

[Yos90] Yoshida, H.: Construction of Higher Order Symplectic Integrators, *Phys. Lett. A*, Vol. 150, pp. 262–268, 1990.

[Yos93] Yoshida, H.: Recent Progress in the Theory and Application of Symplectic Integrators, *Celestial Mechanics and Dynamical Astronomy*, Vol. 56, pp. 27–43, 1993.